Journal Pre-proof

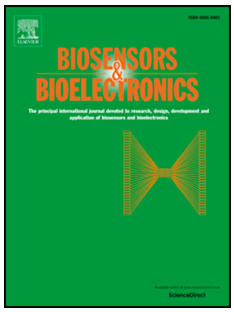

A nanoscale paper-based near-infrared optical nose (NIRON)

Vlad Shumeiko, Yossi Paltiel, Gili Bisker, Zvi Hayouka, Oded Shoseyov

PII: S0956-5663(20)30750-8

DOI: https://doi.org/10.1016/j.bios.2020.112763

Reference: BIOS 112763

To appear in: *Biosensors and Bioelectronics*

Received Date: 12 September 2020

Revised Date: 21 October 2020

Accepted Date: 23 October 2020

Please cite this article as: Shumeiko, V., Paltiel, Y., Bisker, G., Hayouka, Z., Shoseyov, O., A nanoscale paper-based near-infrared optical nose (NIRON), *Biosensors and Bioelectronics* (2020), doi: https://doi.org/10.1016/j.bios.2020.112763.

Author Contributions:

Conceptualization, V.S., O.S., Y.P., Z.H.; Methodology, V.S., O.S., Z.H., G.B., Y.P.; Formal analysis, Software and Investigation V.S.; Validation, V.S., O.S., Z.H.Resources, Z.H., G.B., Y.P., O.S.; Writing—original draft preparation, V.S.; Writing—review and editing, V.S., O.S., Z.H., G.B., Y.P.; Visualization, V.S.; Supervision, O.S.; Project administration, O.S.; Funding acquisition, O.S., G.B., Z.H, Y.P.

A nanoscale paper-based near-infrared optical nose (NIRON)

Vlad Shumeiko[1], Yossi Paltiel[2], Gili Bisker[3], Zvi Hayouka[4],

Oded Shoseyov[1]*

[1] Department of Plant Sciences and Genetics in Agriculture, Faculty of Agriculture, Food and Environment, The Hebrew University of Jerusalem, Rehovot, Israel

[2] Center for Nanoscience and Nanotechnology, Applied Physics Department, The Hebrew University of Jerusalem, Jerusalem, Israel

[3] Department of Biomedical Engineering, Faculty of Engineering, Tel Aviv University, Tel Aviv, Israel

[4] Institute of Biochemistry, Food Science and Nutrition, Faculty of Agriculture, Food and Environment, The Hebrew University of Jerusalem, Rehovot, Israel

* Correspondence: shoseyov@agri.huji.ac.il

Abstract

Electronic noses (e-nose) and optical noses (o-nose) are two emerging approaches for the development of artificial olfactory systems for flavor and smell evaluation. The current work leverages the unique optical properties of semiconducting single-wall carbon nanotubes (SWCNTs) to develop a prototype of a novel paper-based near-infrared optical nose (NIRON). We have drop-dried an array of SWCNTs encapsulated with a wide variety of peptides on a paper substrate and continuously imaged the emitted SWCNTs fluorescence using a CMOS camera. Odors and different volatile molecules were passed above the array in a flow chamber, resulting in unique modulation patterns of the SWCNT photoluminescence (PL). Quartz crystal microbalance (QCM) measurements performed in

parallel confirmed the direct binding between the vapor molecules and the peptide-SWCNTs. PL levels measured before and during exposure demonstrate distinct responses to the four tested alcoholic vapors (ethanol, methanol, propanol, and isopropanol). In addition, machine learning tools directly applied to the fluorescence images allow us to distinguish between the aromas of red wine, beer, and vodka. Further, we show that the developed sensor can detect limonene, undecanal, and geraniol vapors, and differentiate between their smells utilizing the PL response pattern. This novel paper-based optical biosensor provides data in real-time, and is recoverable and suitable for working at room temperature and in a wide range of humidity levels. This platform opens new avenues for real-time sensing of volatile chemical compounds, odors, and flavors.

Keywords: Optical nose; SWCNTs; volatiles; peptides.

Introduction

The human nose is still the primary tool for smell evaluation, especially in the perfume, food, and beverage industries. For example, in the wine industry, one of the main parameters of wine quality is its aroma, with prices of wines often determined by few experts (Cardebat et al., 2014; Cardebat and Livat, 2016). One of the many weaknesses of such an approach was very elegantly demonstrated in a study reported by Morrot et al. (Morrot et al., 2001), in which a white wine artificially colored with an odorless, red dye was olfactory described as a red wine by a panel of 54 tasters; the visual information caused experts to discount olfactory sense. A much less biased system is an obvious need.

Classical analytical methods to detect volatile molecules and monitor their levels, such as ion mobility spectrometry (IMS), gas chromatography (GC), and mass spectrometry (MS), are highly accurate but requires costly equipment and skilled staff, and are time-consuming and unsuitable for real-time monitoring (Paknahad et al., 2019). Currently, most of the commercially available compact and portable volatile sensors rely on conducting polymers and semiconductor metal oxides. Sensor stability over time is one of the major limitations of these systems, with signal drift resulting from sensor degradation, preventing the development of long-term volatile profile databases (Cellini et al., 2017). In addition, the approach usually exhibits low selectivity between different volatiles (Hurot et al., 2019).

In billions of years of evolution, nature has created incredible tools to cope with daily challenges with astonishing effectivity. The human olfactory system orchestrates the smelling task via approximately 400 different types of receptors (Morrison, 2014), which provide the ability to

sense thousands of different smells (or according to some reports; trillions (Bushdid et al., 2014)). Many artificial olfactory systems attempt to mimic the natural approach of the mammalian olfactory system by using a defined set of non-strictly specific receptors to enable the sense of different smells. However, creating a large array of hundreds of artificial sensors is very challenging using current electrochemical approaches, while their replacement in case of degradation is costly and complicated. A more affordable and efficient system should be able to include hundreds of different sensors, while each sensor and the entire array should be easily replaceable in case of degradation. In addition, the sensors must be stable under a wide range of temperatures and humidity levels and provide data in real-time.

Among the five main categories of the biosensors, i.e., electrochemical, optical, piezoelectrical, thermometric, and magnetic (Ali et al., 2017), optical sensors may provide the best solution. In optical biosensors, the detector can be based on a simple camera, and the sensing element does not need to be physically attached to the signal processing system, allowing for remote-sensing and easy sensor replacement. Furthermore, since a single camera can simultaneously detect signals from several sensors, the number of sensors can be scaled up without requiring modification of any hardware elements.

In recent years, carbon nanomaterials have emerged as one of the most promising materials for sensor development, owing to their unique properties, such as chemical stability, mechanical strength, high electrical conductivity, and interesting optical properties (Chen and Chatterjee, 2013; Hendler-Neumark and Bisker, 2019; Jariwala et al., 2013; Kruss et al., 2013; Power et al., 2018). Semiconducting, single-wall carbon nanotubes (SWCNTs) emit photoluminescence (PL) in the near-infrared

region (NIR) (O'Connell et al., 2002), with required excitation wavelength and resulting emission wavelength depending on the chirality of the SWCNTs (Liu et al., 2011). The conductivity, PL intensity, and exact emission wavelengths are dramatically affected by the local environment created by solvents and absorbed molecules as well as by their aggregation state (Choi and Strano, 2007; Larsen et al., 2012; Sanchez et al., 2018). This fascinating feature enables the integration of nanotubes into a variety of optical and electrochemical biosensors for the detection of proteins (Bisker et al., 2018, 2016; Hendler-Neumark and Bisker, 2019; Nelson et al., 2015; Shumeiko et al., 2020; Sobhan et al., 2018) DNA (Clendenin et al., 2007; Weizmann et al., 2011), RNA (Harvey et al., 2019), bacteria (Yamada et al., 2014; Yoo et al., 2016), ions (Forzani et al., 2006), and small molecules (Jeong et al., 2019; Wu et al., 2020). SWCNTs based volatile molecules detection has been demonstrated using variable devices and methods, including electrochemically (Freddi et al., 2019; Penza et al., 2005), reflectometry (Consales et al., 2009), surface acoustic wave (SAW) or using quartz crystal microbalance (QCM) (Penza et al., 2006) and silica optical fiber (Penza et al., 2006). We have recently demonstrated that peptide encapsulated SWCNTs can detect small amounts of acetic acid in wine aroma (Shumeiko et al., 2021). However, to the best of our knowledge, no previous reports suggest using the NIR PL properties of paper based, drop dried peptide-SWCNTs sensors for multiple volatile organic compounds (VOCs) detection and recognition.

SWCNTs are extremely hydrophobic and form insoluble aggregates in water, which quenches their fluorescence (Battigelli et al., 2013). While certain covalent modifications of SWCNT sidewalls may prevent aggregation, the modifications themselves may harm optical properties (Antonucci et al., 2017). Thus, for the development of optical biosensors, noncovalent modifications are usually used for aggregate dispersion. The

main wrapping molecules that are used for SWCNT dispersion are surfactants (Haggenmueller et al., 2008), polymers (Zaumseil, 2019), DNA (Giraldo et al., 2015; Kruss et al., 2017), and peptides (Heller et al., 2011). Peptides are of particular interest as their synthesis is relevantly simple, variable lengths could be chosen, while 21 natural amino acids and a wide range of unnatural amino acids provide an ability to create a huge peptides library. It has been shown that engineering the SWCNT wrapping molecules provides the key for specific analyte recognition (Bisker et al., 2016). SWCNT wrapping molecules and polymers become part of the local environment, thus affecting the intensity and wavelength of the PL emission. Analyte binding directly to SWCNTs or to the wrapping molecule triggers an additional PL change by affecting the SWCNTs themselves, the wrapping molecule, or both (Heller et al., 2011).

Paper is abundant, cost-effective, flexible, disposable, and easy to handle as a substrate where reagents are stored. Furthermore, commercially available inkjet printers are often used for reagent deposition, enabling rapid upscale (Li et al., 2015; Rosati et al., 2019). Paper is widely used for a variety of microfluidic and lateral flow analytical devices (Arduini et al., 2019; Liu et al., 2014). Immobilization of SWCNTs on a paper also was recently demonstrated for the detection of fat-soluble vitamins, and sensor stability for at least 60 days of storage was reported (Salem et al., 2020). However, to the best of our knowledge, there have been no previous reports of the use of paper as a substrate for SWCNT-based NIR artificial olfactory sensor.

The current work reports a development of a novel biosensor based on an array of SWCNTs wrapped with five different peptides and drop-dried on nitrocellulose paper. Different volatile analytes were passed above the array and the PL was continuously recorded with a simple CMOS

camera and analyzed. The developed paper-based NIR optical nose (NIRON) was able to detect and discriminate between different volatile molecules and aromas.

2. Material and Methods

2.1 Chemicals and reagents

Fmoc-AA-OH, 2-(1H-benzotriazole-1-yl)-1,1,3,3-tetramethyluronium hexafluorophosphate (HBTU) and rink amide resin (0.53 mmol/g) were purchased from Chem-Impex (USA). *N*,*N*-dimethylformamide (DMF), diethyl ether, trifluoroacetic acid (TFA), N, N-diisopropylcarbodiimide (DIC), *N*,*N*-diisopropylethylamine (DIEA), and Oxyma Pure were purchased from Biolab, Israel. Polystyrene cuvettes were ordered from Kartell™. Limonene, geraniol, and undecanal were purchased from Sigma (Israel).

2.2 Peptide synthesis

For SWCNT encapsulation, five peptides were synthesized (Supplemental materials, Figure S1). A 30-amino-acid-long helix peptide named HexCoil-Ala, was developed by Grigoryan (Grigoryan et al., 2011), and four aromatic peptides named WFK, WLK, WK, and YH, were developed in our lab. YH (YHHYHHYH) was the shortest tested peptides, consisting of 8 amino acids. The remaining peptides were 20 amino acids long. HexCoil-Ala and YH were synthesized on the CEM Liberty Blue™ Automated Microwave Peptide Synthesizer (Singh and Collins, 2014), on a 0.10 mmol scale, using rink amide resin. Briefly, 10% w/v piperazine was used as the Fmoc-deblocking reagent. Post-deprotection washing with

DMF was followed by coupling, using a 4-fold excess of Fmoc-AA-OH (0.2 M in DMF), Oxyma Pure, and DIC. The peptide was cleaved from the resin by a 3 h incubation, in a solution containing 95% (v/v) TFA, 2.5% (v/v) water, and 2.5% (v/v) triisopropylsilane. The peptide was then precipitated from the solution by the addition of cold ether and harvested by centrifugation (4°C, 5000 RCF). Ether was removed, and the pellet was freeze-dried. The synthesis products were validated by mass spectrometry (MALDI-TOF).

WFK, WLK, and WK were produced as a random mixture, using a previously described (Hayouka et al., 2013; Stern Bauer and Hayouka, 2018) in a MARS VI multimode microwave. Coupling reactions were conducted with combinations of L-Fmoc-protected amino acids. A stock solution containing defined proportions of the amino acids was prepared (0.5:0.5 for WK, 0.25:0.25:0.5 for WLK and WFK). Four equivalents of the amino acid mixture were activated with four equivalents of HBTU and eight equivalents of DIEA in DMF. The activated amino acid mixture was added to the solid-phase synthesis resin, and the reaction mixture was heated to 70°C in a microwave (2-min ramp to 70°C, 4-min hold at 70°C). Fmoc deprotection was achieved by adding 20% piperidine in DMF and heating the solution to 80°C in the microwave (2-min ramp to 80°C, 3-min hold at 80°C).

2.3 Preparation of peptide-encapsulated SWCNTs

Five peptide/SWCNT suspensions were prepared using a protocol published elsewhere, with minor modifications (Heller et al., 2011). Briefly, 4mg of one of the peptides and 4mg SWCNTs (CoMoCAT™ Signis® SG65, Sigma) were mixed in 4 mL distilled water (DW) using a one-eighth-inch probe-tip sonicator, set at 10 W, for 20 min. The resulting

solution was centrifuged twice for 40 min, at 16,000 × g, to remove aggregates, and the supernatant was carefully collected each time. The SWCNT concentration was calculated using Beer-Lambert law (ε_{632} = 0.036 L mg^{-1} cm^{-1} (Kruss et al., 2014)). The peptide-encapsulated SWCNT stock was prepared by diluting the resulted suspension with DW, to 15 mg/L.

2.4 Sensor preparation

A 0.4 μl drop of 15 mg/L peptide-encapsulated SWCNTs was drop-casted on nitrocellulose paper, which was then dried on an aluminum block in an oven with ventilation, under 65°C for 10 min. A custom-made chamber was prepared with inlet and outlet tubes for gas flow experiments.

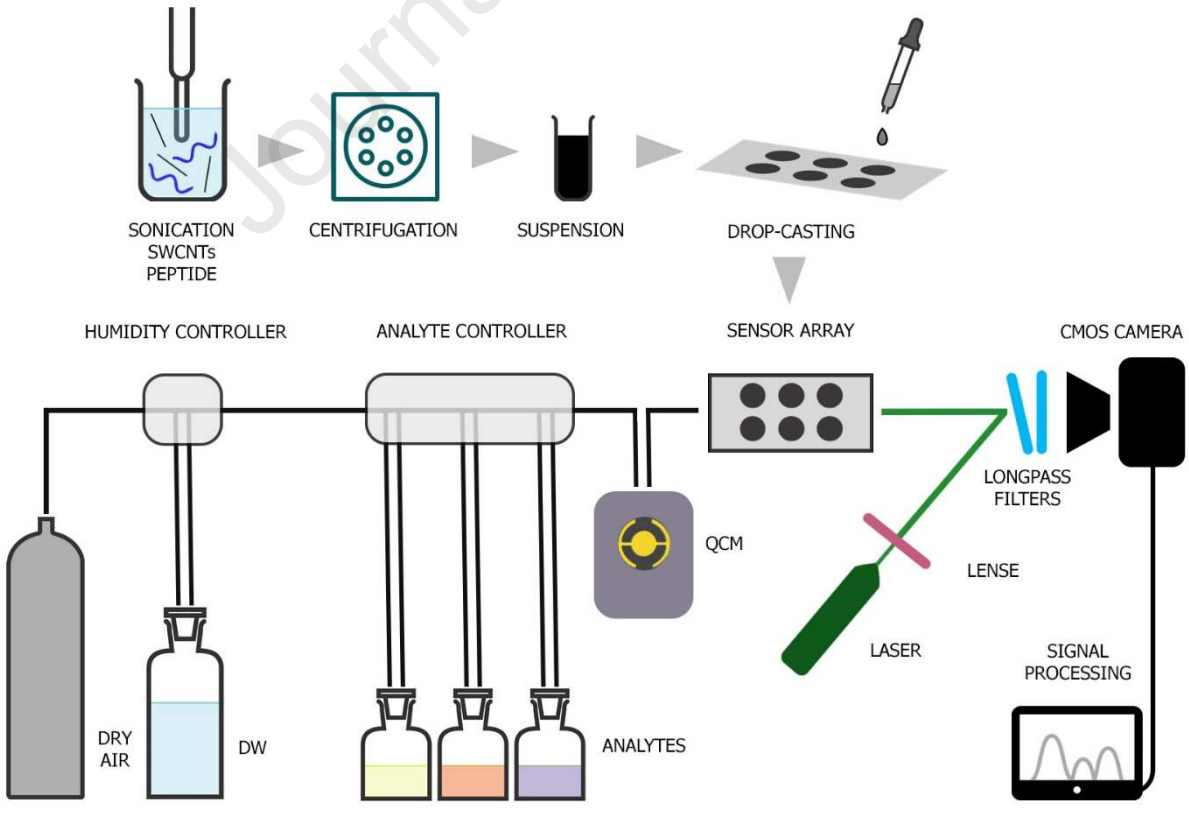

Figure 1: Schematic of the preparation of the sensor, flow control system, QCM, and optical setup.

2.5 Analyte sensing

A custom setup was constructed for analyte sensing (Figure 1). A 532nm laser (100 mW output, PGL-V-H-532 CNI) was used for excitation of the SWCNTs. The PL emission of the drop-dried peptide-encapsulated SWCNTs sensors was continuously recorded using a CMOS camera (XIMEA) with a 950 nm long-pass filter (Thorlabs). The video was processed with custom-built Python software that analyzed PL intensity changes of each sensor (XIMEA API, Anaconda distribution, and OpenCV library (Bradski, 2000)). For intensity measurements, an area in the center of the sensors with the same radius was analyzed in all cases. The 3D PL profile was analyzed using Fiji ImageJ distribution (Schindelin et al., 2012) and the Interactive 3D Surface Plot plugin (Barthel, 2006). Linear discriminant analysis (LDA) was performed using the Scikit-learn python library (Pedregosa et al., 2011). Statistical analysis was performed using GraphPad Prism software version 6.0 for Windows.

Before each experiment, all sensors were allowed to reach a steady-state over 10 min, with clear airflow, under 100 mW laser excitation. Usually, a 45-second analyte flow was followed by 250-second clear airflow, unless indicated otherwise. The relative humidity (RH) of the air in the flow tube was measured with a TFA 30.5013 hygrometer before entering the analyte chamber. To control the RH, a 100% RH airflow was mixed in different proportions with dry airflow before being introduced into the analyte tank. To study the sensor response to various concentrations

of ethanol, clear airflow was mixed in different proportions with airflow containing ethanol vapor and passed above a commercial semiconductor MQ3 sensor (SUKRAGRAHA) before entering to the PDMS chamber. All experiments were carried out under room temperature (23-25°C).

2.6 QCM

A QCM (openQCM Wi2 manufactured by Novaetech S.r.l.) was used to study the binding kinetics of the volatiles to peptide-SWCNTs sensors. Nine 0.4 μl drops of 10 mg/L peptide-encapsulated SWCNTs were drop-casted, side-by-side on the quartz sensor (10 MHz). The drops were dried on an aluminum block in an oven with ventilation, under 65°C, for 10 min. Before analyte screening, the QCM was calibrated with clear airflow (55% RH) for 40 min. Analyte screening was performed as described in section 2.5 and Figure 1.

2.7 Beverage sensing and deep learning

Vodka (40% alcohol), light beer (5% alcohol), and red wine (12.5% alcohol) purchased in a local market were injected (50 ml) into a 1L glass bottle with inlet and outlet tubes. During sensing, clear airflow (55% RH) was passed above the analyte to simulate sniffing and allowed to enter the chamber containing the peptide-encapsulated SWCNTs sensors. An open-source python library ImageA (Olafenwa et al., 2018) was used for machine learning (ML). Three algorithms were tested: ResNet, DenseNet, and Inception. Beverage vapor was passed above the sensors for 90 sec, followed by 6.3 min of clear airflow. Ten pictures were taken from the steady-state region of each sensing cycle. Overall, 350 images were used for training and 120 images for testing.

2.8 Sensing of limonene, geraniol, and undecanal

Analytes (1 mL) were placed in a 1L glass bottle with inlet and outlet tubes. The sensing was performed as described above, with a 45-second analyte flow, followed by 6.3 minutes of clear airflow. The experiment was performed under 55% RH.

3. Results and Discussion

3.1 Sensor design

The (6,5) chirality of the SWCNTs was selected as the basic sensor building block. (6,5) SWCNTs emit PL with a peak at 1000 nm (Chen et al., 2007), enabling the use of a silicon detector-based camera, while most of the other chiralities emit PL at much higher wavelengths, thus requiring indium gallium arsenide (InGaAs) detectors, which are much more expensive, bulky, require extensive cooling and provide lower resolution. To fabricate the array, five peptides were designed and synthesized (Supplemental materials, Figure S1). Four of the peptides were rich in aromatic amino acids, which are known to enhance peptide binding to the sidewalls of SWCNTs via pi-pi interactions (Chen et al., 2013). The fifth peptide. i.e., HexCoil-Ala is a helix peptide without aromatic amino acids that was previously reported (Demir et al., 2018). Three out of four of the aromatic peptides were 20 amino acid long. They were synthesized randomly by incorporating a mixture of amino acids in predefined proportions at each coupling step, instead of a single amino acid. This approach yields mixtures containing up to 2^{20} different peptides when using two types of amino acids, and 3^{20} when incorporating three amino acids (Topman et al., 2018). This approach was expected to increase the chances for a sensitive and robust response by increasing peptides variability. Moreover, peptide mixtures are simpler and cheaper to

synthesize than specific sequence peptides while still enabling reproducibility (Hayouka et al., 2013). The fifth aromatic peptide was a 7-mer peptide with a defined sequence of YHHYHHYH. Taken together, the array contained peptides with wide variability in their composition, length, and interaction mechanism with the SWCNT wall. All five peptides successfully wrapped SWCNTs after sonication and dispersed them in the water, as could be seen in the UV-VIS spectrum (Supplemental materials, Figure S2). The peptide-SWCNTs suspension was found to be stable for more than one year at 4 °C. The resulting peptide-encapsulated SWCNTs composites were drop-dried side-by-side on nitrocellulose paper to create the sensor array, where each dot was comprised of a different peptide-SWCNTs composite.

3.2 Sensors reaction to ethanol vapor

Next, the reaction of the prepared sensors to volatiles was evaluated. The first tested analyte was a solution of 10% v/v ethanol in water. To simulate the sniffing of a solution, clear air was passed above the ethanol solution before entering the sensor chamber. As seen in Figure 2A, each of the sensors responded differently to the ethanol vapor. While all five sensors showed increased PL intensity after analyte flow, both the kinetics and the final intensity were significantly different. WLK, HelixCoil-Ala, and YH sensors reached a plateau in PL after approximately 24 sec from the start of the analyte flow, while the PL of WFK and WK sensors continued to rise even after 45 sec. The recovery rate upon passage of clear airflow through the chamber was also different; for example, even though the WK sensor showed a greater change in PL, it recovered slightly faster than the WFK sensor. The overall recovery took around 160 sec; however, it could have potentially been enhanced by increasing airflow or

by heating the sensors.

As one of the motivations behind drying sensors was to avoid the diffusion of the analyte from the air to the liquid, the responsiveness of wet sensors was assessed. To this end, the nitrocellulose paper with the sensors was mounted on top of a hydrated PVA hydrogel, such that the sensors remained wet during the airflow. Wet sensors were indeed significantly less sensitive to the 10% v/v ethanol vapor, indicating that dry sensors

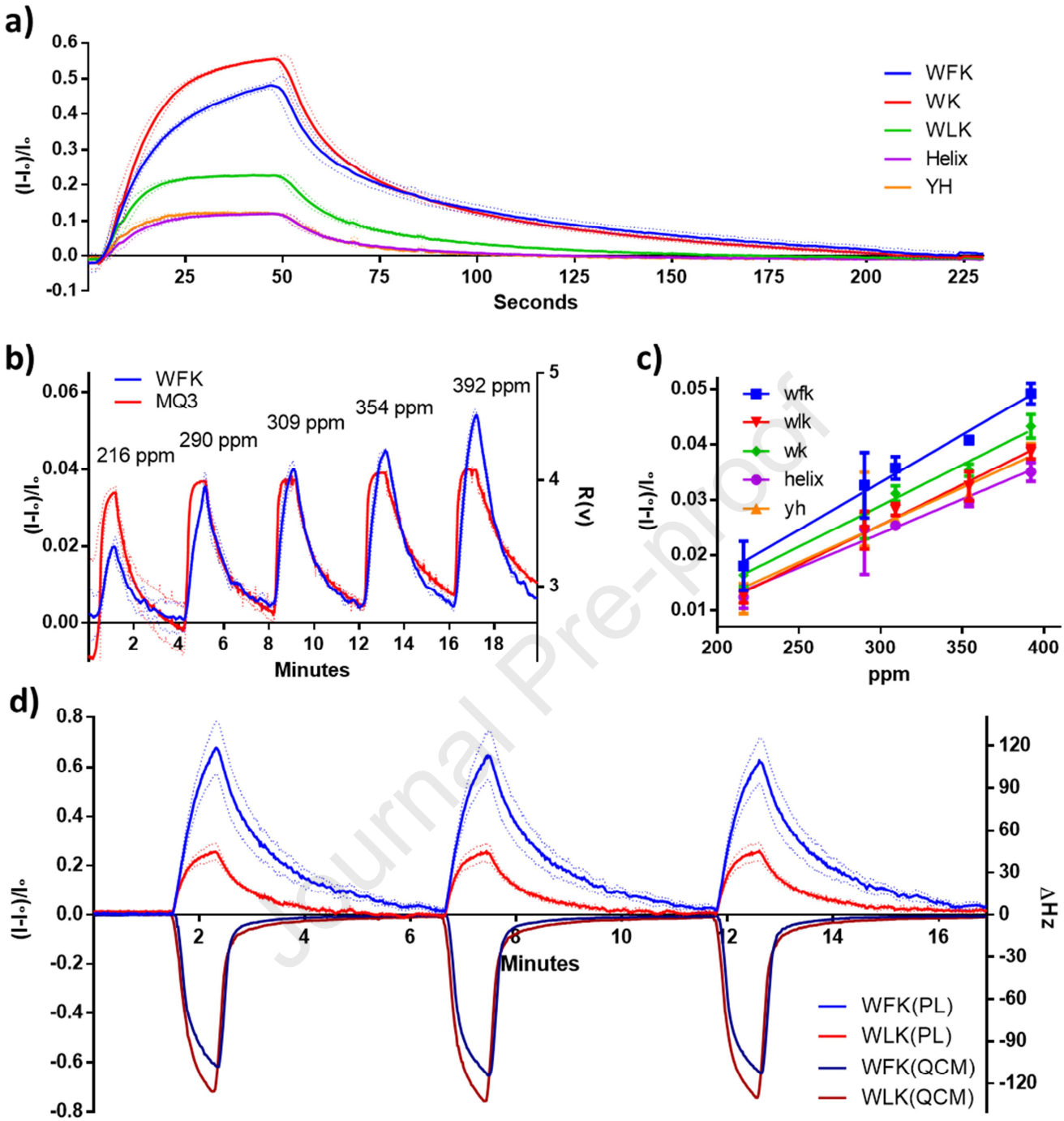

Figure 2: Response of peptide-encapsulated SWCNT sensors to ethanol vapor. A) Change in photoluminescence of five sensors in response to the vapor of a 10% v/v ethanol solution passed above the sensors for 45 seconds, followed up by a flow of clear air (n=4). B) The WFK sensor response to 216 ppm, 290 ppm, 309 ppm, 354 ppm, and 392 ppm ethanol in the airflow. The red line represents a commercial semiconductor sensor

(MQ3) response, which served as a control (n=3). C) Linear graphs presenting the dependence of the sensor PL on ethanol concentration (n=3). Linear equation and linear correlation coefficient could be found in supplemental materials, Table S1. D) WFK and WLK sensor responses to 10% v/v ethanol vapor, passed over the sensors, followed by clear airflow, as measured using coupled optical and QCM sensors. Error bars and dashed lines represent the standard deviation (n=3).

significantly boost sensitivity (Supplemental materials, Figure S4).

Next, the sensitivity of drop-dried peptide-encapsulated SWCNTs sensors to different concentrations of ethanol was evaluated. The PL of the WFK sensor increased linearly with increasing concentrations of the ethanol vapor (Figure 2 B-C). The developed biosensor showed a limit of detection around 216 ppm of ethanol. A similar linear response was observed for the other sensors as well (Figure 2C).

In order to gain insight into the sensing mechanism, the binding kinetics and the optical response were simultaneously recorded by passing the 10% v/v ethanol solution vapor over a QCM module immediately before entering the optical chamber (Figure 1). Upon analyte introduction, the QCM sensor showed a graduate decrease in a signal, indicating analyte binding to the peptide-SWCNTs composite, while the optical sensors showed a simultaneous increase in PL (Figure 2D). After the introduction of the clear airflow, graduate analyte release was observed, with full recovery of QCM and optical sensors. The QCM sensors responded faster and recovered faster than optical sensors, and this could be explained by the chamber geometry. The QCM chamber is very narrow; thus, the flow speed of the analyte and of the clear air is fast. In contrast, the PDMS chamber used for optical sensing is much wider; thus, the flow

is slower, as was the response. Interestingly, WFK-QCM sensors were less reactive to the ethanol vapor as compared to the WLK-QCM sensor, while the optical response of WFK was more than three-fold higher than that of WLK. These findings indicate that the total bound amount of analyte was not the only determinant of the strength of the optical response.

As humidity is a highly dynamic environmental parameter, which may pose challenges to artificial nose systems, sensor response to ethanol vapor under different humidity levels was assessed. Humidity levels had a minor impact on the final PL intensity in response to the vapor of 10% v/v ethanol of most of the sensors (Supplemental materials, Figure S5). The WK and WLK sensors were the most affected. For example, the WK sensor showed an 8% decrease in the response under 30% RH and 3% increase under 98% RH as compared to the response under RH of 65%. Interestingly, although the final PL intensity of the sensors after ethanol sensing was not significantly impacted by RH, their baseline PL levels were profoundly affected by humidity (Supplemental materials, Figure S6 B). These results could be explained by the fact that water molecules bind to the SWCNTs surface (as was demonstrated using QCM (Supplemental materials, Figure S7)) and affect sensors PL (Figure S6 A) in a similar way to other analytes.

The long-term stability of the sensors was evaluated. 10% v/v ethanol vapor sensing was performed continuously for 10 h. Overall, more than 70 cycles of ethanol sensing, followed by clear airflow, were performed. An increase in baseline PL of the sensors was noted with time, with no significant change in the peak height relative to the baseline level of the recent cycle (Supplemental materials, Figure S8). These results suggest that the sensors could potentially be used continuously for many sensing cycles. Moreover, as the sensors are deposited on a paper, the array can be easily replaced. Considering that each sensor dot required as

little as 5 ng SWCNTs, sensor replacement would be very cost-effective.

3.3 Sensor reaction to alcohols

The results above indicated that there is an optical response of drop-dried sensors toward ethanol vapor, with each of the sensors reacting differently, thus producing a rich optical fingerprint. Sensory capacity to generate distinct optical patterns for other alcohols was then assessed by exposing them to methanol, propanol, and isopropanol 10% v/v solutions vapors. The selected molecules are structurally similar, rendering them a worthy means of determining the discriminatory abilities of the sensors. The response of the sensors to the vapors of the solutions was recorded for two-hours. In each cycle, vapor was introduced and then cleared out with clear airflow. The sensors showed a remarkable recovery after each cycle (Figure 3A), with the baseline and peak PL heights remaining stable throughout the experiment.

The observed PL changes (Figure 3 B-F) revealed that as with ethanol vapor, each sensor responded differently to the analytes. While WK, WLK, and YH failed to distinguish between ethanol and isopropanol, WFK and Helix enabled their discrimination. All sensors showed a high response to propanol and low response to methanol. The overall reaction of WK and WFK sensors to alcohol was strongest, followed by WLK, YH, and then HelixCoil-Ala. LDA (Figure 3 G) of the responses of all five sensors showed clear discrimination between the four tested analytes, despite their structural similarity. Moreover, sensors were able to discriminate a mixture of ethanol and methanol as well (Supplemental materials, Figure S9).

Few distinct mechanisms accounting for PL modulation of SWCNT have been identified to date that may explain the observed phenomena. It includes; Fermi level shift caused by an analyte's adsorption with a

448 favorable reduction potential (Barone et al., 2005; Heller et al., 2011),
449 exciton quenching caused by an analyte that perturbs the exciton itself

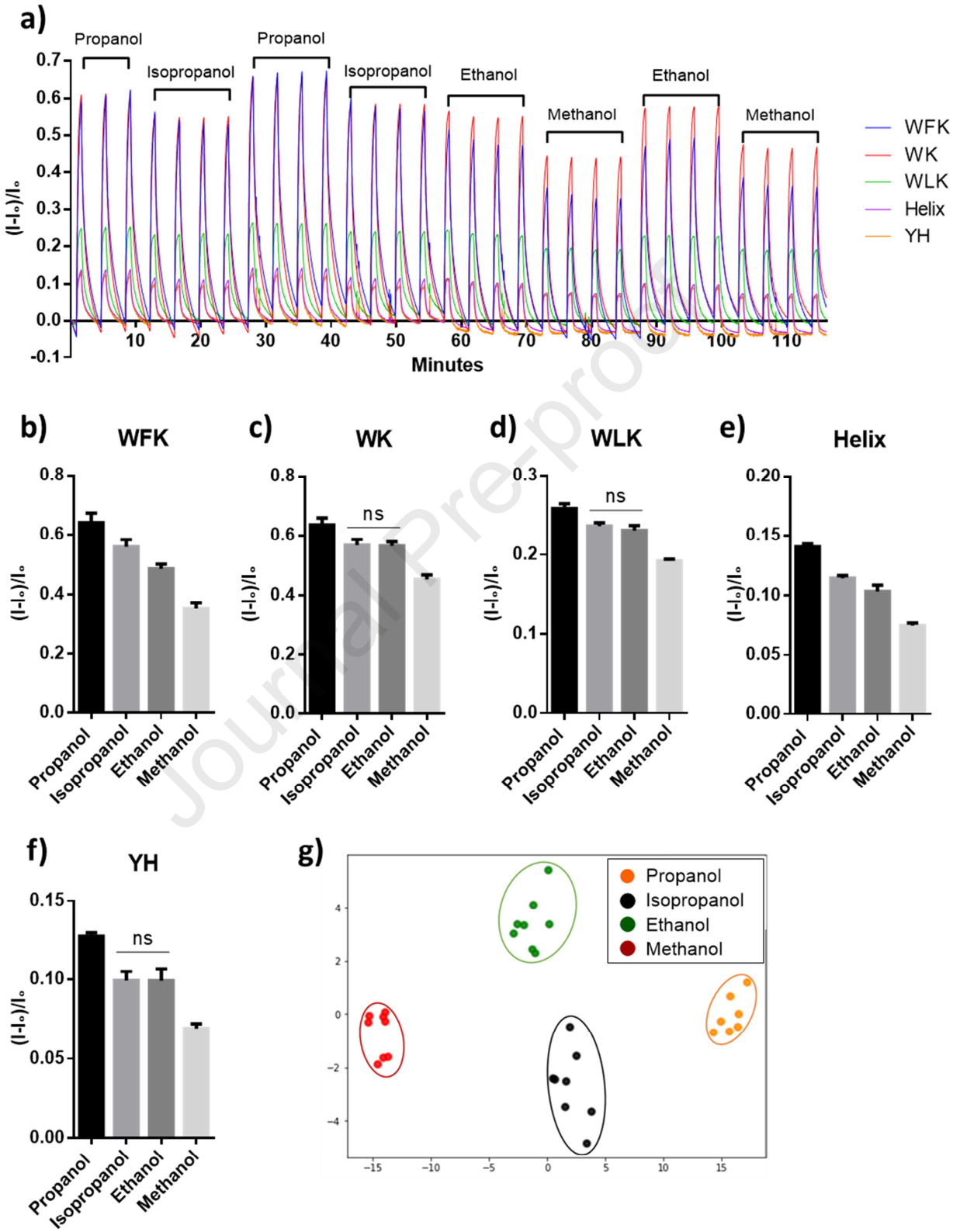

450

Figure 3: Optical response of the sensor to five alcohols 10% v/v solutions; ethanol, methanol, propanol, and isopropanol. A) Two hours experiment where each peak represents changes in PL after reaction to one of the analytes following by recovery with clear air. B-F) A summary of the relative PL change of the sensors after reaction to each analyte. Data are presented as mean. Error bars represent standard deviation. n=8. P<0.05 unless otherwise indicated. G) LDA of peptide-encapsulated SWCNTs sensors PL responses to 10% v/v analytes solutions.

(Barone et al., 2005; Heller et al., 2011), or solvatochromic shifting caused by perturbing an encapsulating peptide, thereby changing the accessibility of the SWCNT surface to other molecules (Choi and Strano, 2007; Heller et al., 2011). Selectivity can be imparted to the above mechanisms by carefully designing wrapping molecules to affect or block the analyte's binding ability to the SWCNT walls (Heller et al., 2011). Interaction with the analytes may also change the SWCNT's accessibility to specific moieties on the encapsulating peptides or the nitrocellulose paper or water vapors, thus affecting PL.

Interestingly, there is a strong negative correlation between the analytes' vapor pressure (Supplemental materials; Table S2) and the PL response (Supplemental materials; Table S3 and Figure S10). The PL response of all sensors was high to propanol vapor while low to methanol vapor. In WFK, WLK and Helix response to isopropanol was higher than to ethanol, while in WK and YH sensors, there was no difference in PL response between these two analytes. The analytes' vapor pressure displays the opposite trend, with ethanol and isopropanol having the smallest difference. Methanol vapor pressure is 12.9 kPa, followed by ethanol 5.95kPa and isopropanol 4.24 kPa. Propanol has the lowest vapor

pressure of 1.9 kPa ("Dortmund Data Bank," 2020). Higher vapor pressure could mean that more molecules stay in the gas phase and less likely to accumulate on the SWCNTs' surface. This fact could explain the similar pattern of the response of the sensors.

The binding kinetics of the alcohols to the different sensors was then assessed using the previously mentioned QCM technique. Four sensors (WFK, WLK, WK, and YH) were drop-dried separately on the QCM crystal, and vapor of different analytes was passed over it, with intermittent clean air washes. Except for YH, which displayed a minor drift, the rest of the sensors presented a sufficiently stable recovery to baseline levels after each cycle (Figure 4 A-D). Using only the QCM data and performing LDA analysis also enabled discrimination between all four volatiles (Figure 4G).

Both the PL response and QCM measurements demonstrate that sensors have a similar pattern toward different analytes, suggesting once again that analytes bind mainly directly to SWCNTs while peptides may block specific binding sites. However, it is challenging to compare QCM response to the optical response. First of all, the QCM has a very narrow chamber; thus, the analyte flow in the QCM is much faster. Moreover, the substrate surface is very different; while in QCM, the sensors were dried on a flat gold surface, during optical measurements, the sensors were drop-dried on a paper. The paper has a significantly larger surface volume; thus, the dried dot's geometry is entirely different.

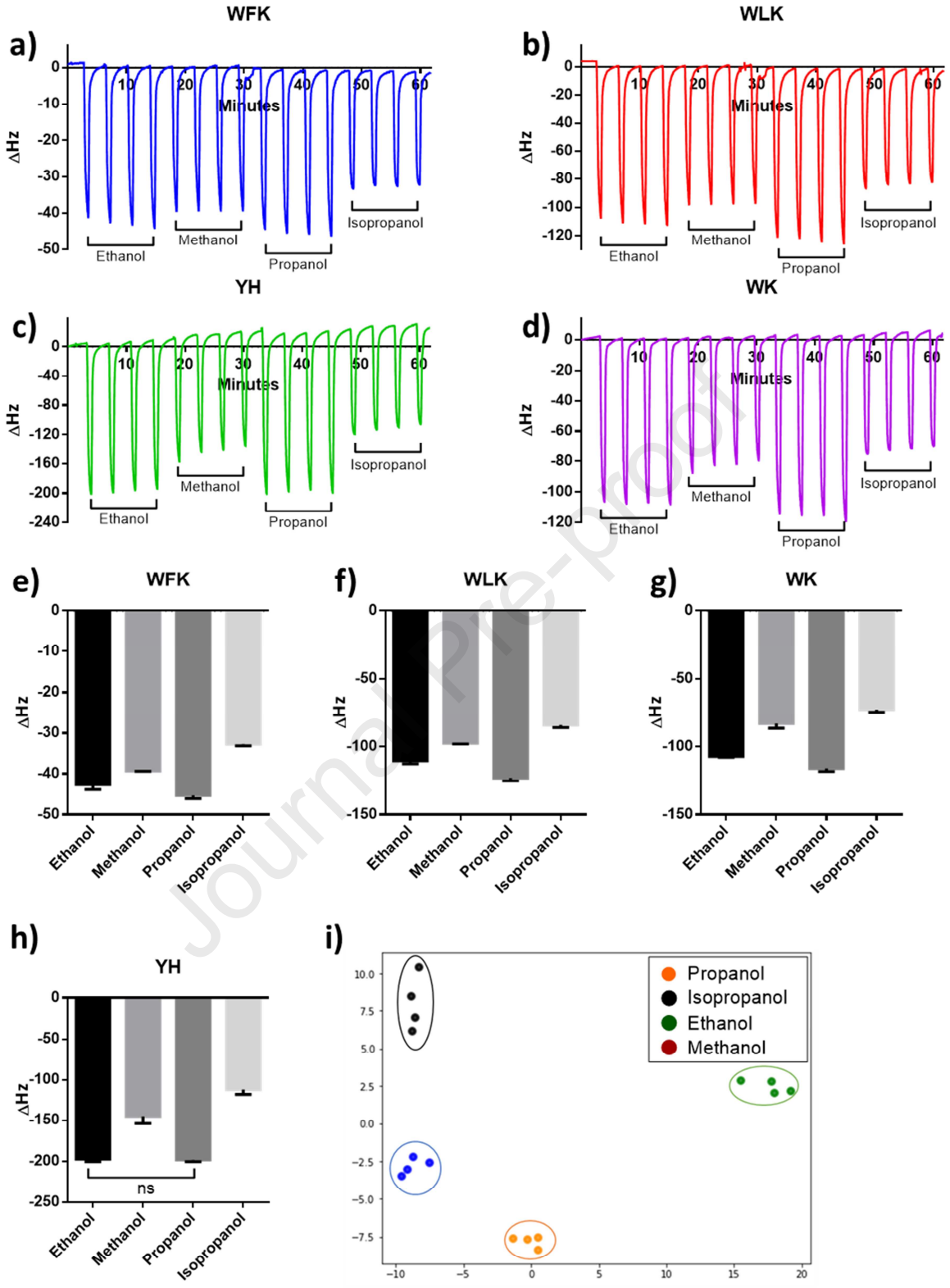

Figure 4: Response of the QCM crystal with a drop-dried peptide-encapsulated SWCNTs sensors to vapors of 10% v/v solution of ethanol,

methanol, propanol, and isopropanol. Four peptides were tested: WFK, WLK, YH, and WK. A-D) A one-hour experiment where each peak is representing the change in Hz after the passage of analyte vapor, followed by the passage of clear air. E-H) A summary of the change in frequency of each of the sensors after exposure to each of the four analytes. Error bars represent standard deviation. n=4. P<0.05 unless otherwise indicated. I) LDA.

3.4 Beverage aroma sensing using machine learning

Continuously analyzing sensors intensity changes during analyte flow relative to the baseline is one of the possible ways to discriminate between analytes. Another approach is to teach the system to recognize analytes by analyzing a picture of all sensors together, exactly in the way that ML can differentiate between cats and dogs. Moreover, this enables analytes discrimination without requiring any preprocessing or continuous monitoring. To this end, deep learning was harnessed to train the NIRON device to recognize the smells of wine, beer, and vodka.

First, the kinetics of the PL responses were analyzed. The overall response of the sensors (Figure 5 A-D) was in correlation with ethanol percentage, with the highest response observed with vodka (40% ethanol), followed by wine (12.5%), and then by beer (4%). However, sensors responses to wine aroma were higher than to water containing 12.5% ethanol (Supplemental materials, Figure S12), indicating that other volatile molecules in wine also affect sensors PL. LDA of the response of all sensors demonstrated that they were able to clearly discriminate between the beverages (Figure 5 E). Interestingly, the kinetics of the PL response was significantly different between the analytes. For example, while the response to vodka was the highest among the analytes, most of the

sensors

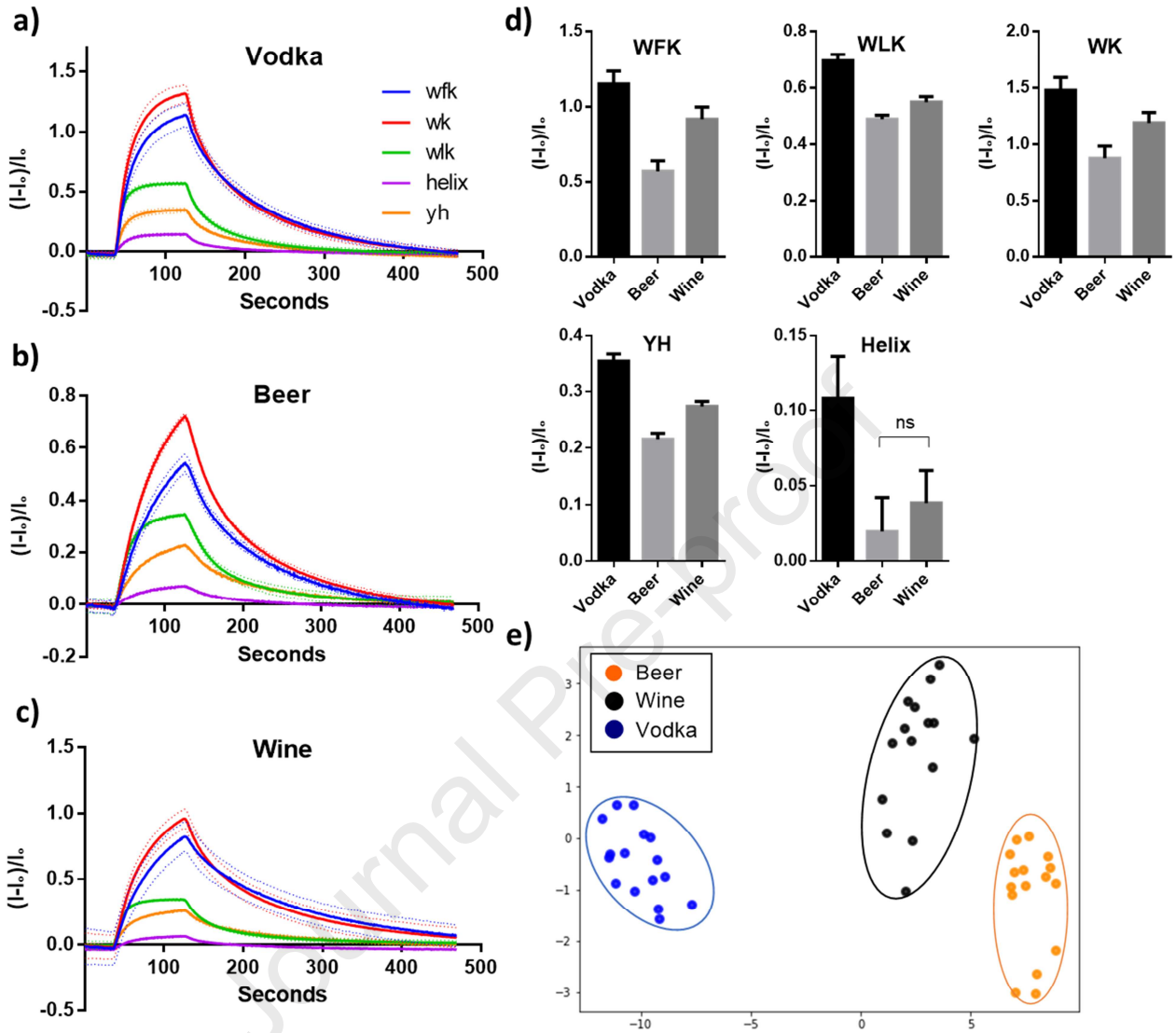

Figure 5: The dynamic response of peptide-SWCNTs sensors to different beverages followed by clear airflow. Figures present changes in PL in response to vodka (A), beer (B), and wine (C) vapors. D) A summary of the relative PL change of the sensors after reaction to Beer, Wine, or Vodka. Data are presented as mean. Error bars represent standard deviation. n=16. P<0.05 unless otherwise indicated. E) LDA of the response of the sensor.

reach a plateau at the end of the experiment. However, during the sniffing

of beer, the response of the sensors was lower and slower, and most of the sensors did not reach a plateau. Further analysis of the kinetics of PL may provide additional data for analytes discrimination.

Machine learning using the ResNet, DenseNet, and Inception deep learning neural networks were performed. Unprocessed images of the array during the sensing of each analyte were fed to the models (Supplemental materials, Figure S13). The learning curve is detailed in supplemental materials, Figure S14. Among these three networks, ResNet showed the best performance and was able to find several models with high accuracy, indicating that array images could be used for analytes classification.

3.5 Reaction of the NIRON sensor to limonene, geraniol, and undecanal

To test whether the sensors can react to other volatiles, they were exposed to vapors of limonene, geraniol, and undecanal. Limonene is a monocyclic monoterpene with a lemon-like odor that is widely used as a flavor in perfumes, soaps, foods, and beverages (Sun, 2007). Geraniol is a terpene that is widely used in the flavor and fragrance industries (Chen and Viljoen, 2010). Undecanal is an eleven-carbon aldehyde that is used in perfumes (Indradas et al., 2014). The sensors array readily detected all three molecules in the airflow and efficiently differentiated between them (Figure 6). The response of all sensors was significantly higher to limonene than to geraniol and undecanal (Supplemental materials, Figure S15), suggesting that the aromatic structure of limonene improves its interaction with the sensor.

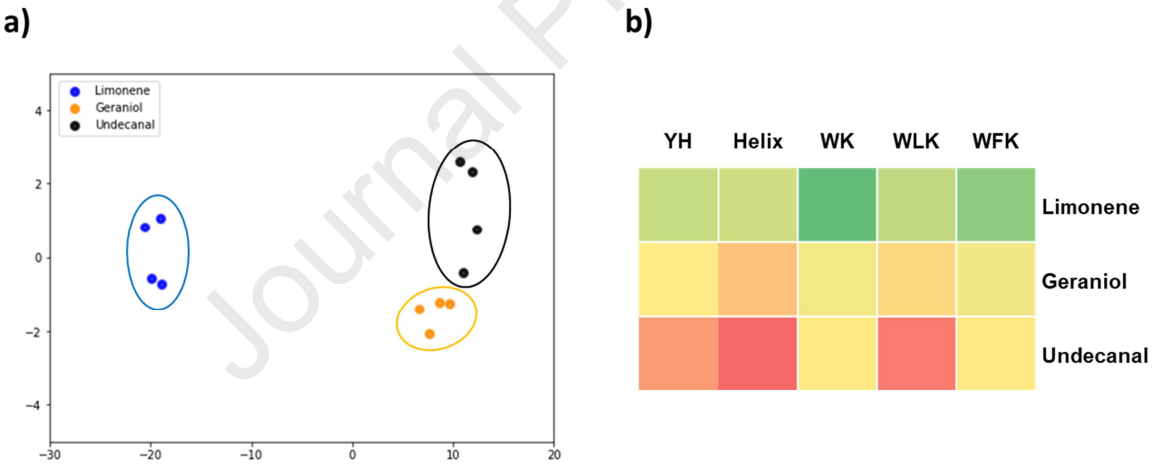

Figure 6: Response of peptide-SWCNTs sensors to the vapors of limonene, geraniol and undecanal. A) LDA and B) Heat map presentation of the photoluminescence changes of the sensors upon exposure to limonene, geraniol and undecanal.

4. Conclusion

In this work, we developed a prototype of a real-time, room temperature, paper-based artificial NIR optical biosensor comprised of an array of drop-casted peptide-wrapped SWCNTs. We have established a simple optical setup, where (6,5) SWCNT chirality was used to reduce system costs and complexity, as its emission wavelengths enable the use of a silicon-based camera. PL response of the sensors to different volatiles in the gas phase at room temperature was monitored. Each tested analyte produced a different optical response of the array, thus enabling discrimination between the volatiles. QCM measurements were performed in parallel and confirmed the direct binding between the analytes and SWCNTs/peptide complex. We have also demonstrated that the sensor array signal may be analyzed using a machine learning algorithm directly from the resulted image of the entire array without the need to analyze each sensor separately. As a signal drift is a well-known phenome in various gas sensors, we have deposited our array on a paper that is

physically separated from the detector; therefore, sensors replacement in case of degradation is simple and cost-effective.

The presented technique opens numerous possibilities of sensing and analyzing a wide range of smells and complex aromas to be used in various applications.

References

Ali, J., Najeeb, J., Asim Ali, M., Farhan Aslam, M., Raza, A., 2017. J. Biosens. Bioelectron. 08, 1-9.

Antonucci, A., Kupis-Rozmysłowicz, J., Boghossian, A.A., 2017. ACS Appl. Mater. Interfaces 9.13 (2017): 11321-11331

Arduini, F., Cinti, S., Caratelli, V., Amendola, L., Palleschi, G., Moscone, D., 2019. Biosens. Bioelectron. 126, 346–354.

Barbosa, A.J., Rita Oliveira, A., Roque, A.C., 2018. Trends Biotechnol, 36(12), 1244-1258.

Barone, P.W., Baik, S., Heller, D.A., Strano, M.S., 2005. Nat. Mater, 4(1), 86-92.

Barthel, K.U. Proceedings of the ImageJ Conference, Luxembourg, 18–19 May 2006

625 Battigelli, A., Ménard-Moyon, C., Da Ros, T., Prato, M., Bianco,
626 A., 2013. Adv. Drug Deliv. Rev, 65(15), 1899-1920.
627 Bisker, G., Bakh, N.A., Lee, M.A., Ahn, J., Park, M., O'Connell,
628 E.B., Iverson, N.M., Strano, M.S., 2018. ACS Sensors 3,
629 367–377.
630 Bisker, G., Dong, J., Park, H.D., Iverson, N.M., Ahn, J., Nelson,
631 J.T., Landry, M.P., Kruss, S., Strano, M.S., 2016. Nat.
632 Commun. 7, 1–14.
633 Bradski, 2000. Dr Dobb's J. Softw. Tools 25, 120–125.
634 Bushdid, C., Magnasco, M.O., Vosshall, L.B., Keller, A., 2014.
635 Science, 343(6177), 1370-1372.
636 Cardebat, J.-M., Figuet, J.-M., Paroissien, E., 2014. JWE, 9(3),
637 282.
638 Cardebat, J.M., Livat, F., 2016. Int. J. Wine Bus. Res. 28, 43–
639 58.
640 Cellini, A., Blasioli, S., Biondi, E., Bertaccini, A., Braschi, I.,
641 Spinelli, F., 2017. Sensors, 17(11), 2596.
642 Chen, A., Chatterjee, S., 2013. Chem. Soc. Rev. 42, 5425–
643 5438.
644 Chen, W., Viljoen, A.M., 2010. South African J. Bot. 76, 643–
645 651.
646 Chen, X., Yu, X., Liu, Y., Zhang, J., 2013. J. Mol. Graph. Model.

46, 83–92.

Chen, Y., Wei, L., Wang, B., Lim, S., Ciuparu, D., Zheng, M., Chen, J., Zoican, C., Yang, Y., Haller, G.L., Pfefferle, L.D., 2007. ACS Nano 1, 327–336.

Choi, J.H., Strano, M.S., 2007. Appl. Phys. Lett. 90, 223114.

Clendenin, J., Kim, J.W., Tung, S., 2007, IEEE Conference. 2007. pp. 1028–1033.

Consales, M., Crescitelli, A., Penza, M., Aversa, P., Veneri, P.D., Giordano, M., Cusano, A., 2009. Sensors Actuators, B Chem. 138, 351–361.

Demir, K., Alıcı, H., Yaşar, F., 2018. Chinese J. Phys. 56, 46–57.

Dortmund Data Bank. Oldenburg. http://www. ddbst. com (accessed 5.09.20).

Forzani, E.S., Li, X., Zhang, P., Tao, N., Zhang, R., Amlani, I., Tsui, R., Nagahara, L.A., 2006. Small 2, 1283–1291.

Freddi, S., Drera, G., Pagliara, S., Goldoni, A., Sangaletti, L., 2019. Analyst 144, 4100–4110.

Giraldo, J.P., Landry, M.P., Kwak, S.-Y., Jain, R.M., Wong, M.H., Iverson, N.M., Ben-Naim, M., Strano, M.S., 2015. Small 11, 3973–3984.

Grigoryan, G., Kim, Y.H., Acharya, R., Axelrod, K., Jain, R.M., Willis, L., Drndic, M., Kikkawa, J.M., DeGrado, W.F., 2011.

669 Science, 332(6033), 1071-1076.
670 Haggenmueller, R., Rahatekar, S.S., Fagan, J.A., Chun, J.,
671 Becker, M.L., Naik, R.R., Krauss, T., Carlson, L., Kadla, J.F.,
672 Trulove, P.C., Fox, D.F., DeLong, H.C., Fang, Z., Kelley, S.O.,
673 Gilrnan, J.W., 2008. Langmuir 24, 5070–5078.
674 Harvey, J.D., Baker, H.A., Ortiz, M. V., Kentsis, A., Heller, D.A.,
675 2019. ACS Sensors 4, 1236–1244.
676 Hayouka, Z., Chakraborty, S., Liu, R., Boersma, M.D.,
677 Weisblum, B., Gellman, S.H., 2013. J. Am. Chem. Soc. 135,
678 11748–11751.
679 Heller, D.A., Pratt, G.W., Zhang, J., Nair, N., Hansborough, A.J.,
680 Boghossian, A.A., Reuel, N.F., Barone, P.W., Strano, M.S.,
681 2011. Proc. Natl. Acad. Sci. U. S. A. 108, 8544–8549.
682 Hendler-Neumark, A., Bisker, G., 2019. Sensors (Switzerland).
683 Hurot, C., Brenet, S., Buhot, A., Barou, E., Belloir, C., Briand, L.,
684 Hou, Y., 2019. Biosens. Bioelectron. 123, 230–236.
685 Indradas, B., Hansen, C., Palmer, M., Womack, G.B., 2014.
686 Flavour Fragr. J. 29, 313–323.
687 Jariwala, D., Sangwan, V.K., Lauhon, L.J., Marks, T.J., Hersam,
688 M.C., 2013. Chem. Soc. Rev. 42, 2824–2860.
689 Jeong, S., Yang, D., Beyene, A.G., Del Bonis-O'Donnell, J.T.,
690 Gest, A.M.M., Navarro, N., Sun, X., Landry, M.P., 2019. Sci.

691 Adv. 5, 3771–3789.
692 Kruss, S., Hilmer, A.J., Zhang, J., Reuel, N.F., Mu, B., Strano,
693 M.S., 2013. Adv. Drug Deliv. Rev. 65(15), 1933-1950.
694 Kruss, S., Landry, M.P., Vander Ende, E., Lima, B.M.A., Reuel,
695 N.F., Zhang, J., Nelson, J., Mu, B., Hilmer, A., Strano, M.,
696 2014. J. Am. Chem. Soc. 136, 713–724.
697 Kruss, S., Salem, D.P., Vuković, L., Lima, B., Ende, E. Vander,
698 Boyden, E.S., Strano, M.S., 2017. Proc. Natl. Acad. Sci. U.
699 S. A. 114, 1789–1794.
700 Larsen, B.A., Deria, P., Holt, J.M., Stanton, I.N., Heben, M.J.,
701 Therien, M.J., Blackburn, J.L., 2012. J. Am. Chem. Soc. 134,
702 12485–12491.
703 Li, J., Rossignol, F., Macdonald, J., 2015. Lab Chip 15, 2538–
704 2558.
705 Liu, B., Du, D., Hua, X., Yu, X.-Y., Lin, Y., 2014. Electroanalysis
706 26, 1214–1223.
707 Liu, H., Nishide, D., Tanaka, T., Kataura, H., 2011. Nat.
708 Commun. 2, 1–8.
709 Morrison, J., 2014. Nature News.
710 Morrot, G., Brochet, F., Dubourdieu, D., 2001. Brain Lang. 79,
711 309–320.
712 Nelson, J.T., Kim, S., Reuel, N.F., Salem, D.P., Bisker, G., Landry,

M.P., Kruss, S., Barone, P.W., Kwak, S., Strano, M.S., 2015. Anal. Chem. 87, 8186–8193.

O'Connell, M.J., Bachilo, S.H., Huffman, C.B., Moore, V.C., Strano, M.S., Haroz, E.H., Rialon, K.L., Boul, P.J., Noon, W.H., Kittrell, C., Ma, J., Hauge, R.H., Weisman, R.B., Smalley, R.E., 2002. Science 297, no. 5581 (2002): 593-596.

Olafenwa et all., 2018, https://github.com/OlafenwaMoses/ImageAI (accessed 8.9.20).

Paknahad, M., Mcintosh, C., Hoorfar, M., 2019. Sci. Rep. 9, 1–11.

Pedregosa, Fabian, Gaël Varoquaux, Alexandre Gramfort, Vincent Michel, Bertrand Thirion, Olivier Grisel, Mathieu Blondel et al. 2011, J. Mach. Learn. Res. 12: 2825-2830.

Penza, M., Cassano, G., Aversa, P., Antolini, F., Cusano, A., Consales, M., Giordano, M., Nicolais, L., 2005. Sensors and Actuators, B: Chemical. Elsevier, pp. 171–180.

Penza, M., Cassano, G., Aversa, P., Cusano, A., Consales, M., Giordano, M., Nicolais, L., 2006. IEEE Sens. J. 6, 867–874.

Power, A.C., Gorey, B., Chandra, S., Chapman, J., 2018. Nanotechnol. Rev. 7, no. 1: 19-41.

Rosati, G., Ravarotto, M., Sanavia, M., Scaramuzza, M., De Toni, A., Paccagnella, A., 2019. Sens. Bio-Sensing Res. 26, 100308.

Salem, D.P., Gong, X., Liu, A.T., Akombi, K., Strano, M.S., 2020. Anal. Chem. 92, 916–923.

Sanchez, S.R., Bachilo, S.M., Weisman, R.B., 2018. J. Phys. Chem. C 122, 26251–26259.

Schindelin, J., Arganda-Carreras, I., Frise, E., Kaynig, V., Longair, M., Pietzsch, T., Preibisch, S., Rueden, C., Saalfeld, S., Schmid, B., Tinevez, J.Y., White, D.J., Hartenstein, V., Eliceiri, K., Tomancak, P., Cardona, A., 2012. Nat. Methods. A, 676-682.

Shumeiko, V., Malach, E., Helman, Y., Paltiel, Y., Bisker, G., Hayouka, Z., Shoseyov, O., 2021. Sensors Actuators, B Chem. 327, 128832.

Shumeiko, V., Paltiel, Y., Bisker, G., Hayouka, Z., Shoseyov, O., 2020. Sensors 20, 5247.

Singh, S.K., Collins, J.M., 2014. Organic letters. 16(3), 940-943.

Sobhan, A., Oh, J.H., Park, M.K., Kim, S.W., Park, C., Lee, J., 2018. Korean J. Chem. Eng. 35, 172–178.

Stern Bauer, T., and Hayouka, Z. 2018. Journal of Peptide Science 24.7: e3088.

Sun, J. 2007. Alternative Medicine Review, 12(3), 259.

Topman, S., Tamir-Ariel, D., Bochnic-Tamir, H., Stern Bauer, T., Shafir, S., Burdman, S., Hayouka, Z., 2018. Microb. Biotechnol. 11, 1027–1036.

Weizmann, Y., Chenoweth, D.M., Swager, T.M., 2011. J. Am. Chem. Soc. 133, 3238–3241.

Wu, H., Nißler, R., Morris, V., Herrmann, N., Hu, P., Jeon, S.J., Kruss, S., Giraldo, J.P., 2020. Nano Lett. 20, 2432–2442.

Yamada, K., Kim, C.-T., Kim, J.-H., Chung, J.-H., Lee, H.G., Jun, S., 2014. PLoS One 9, e105767.

Yoo, S.M., Baek, Y.K., Shin, S., Kim, J.H., Jung, H.T., Choi, Y.K., Lee, S.Y., 2016. J. Nanosci. Nanotechnol. 16, 6520–6525.

Zaumseil, J., 2019. Adv. Electron. Mater. 5, 1800514.

Highlights

- An optical nose based on drop-dried peptide encapsulated SWCNTs was developed.
- An array of five sensors was deposited on a paper. The developed sensor was able to discriminate between various volatile molecules.
- The developed sensor is fully recoverable, stable for hours of continuous work, could operate at room temperature and under a wide range of humidity conditions.

Declaration of interests

☒ The authors declare that they have no known competing financial interests or personal relationships that could have appeared to influence the work reported in this paper.

☐The authors declare the following financial interests/personal relationships which may be considered as potential competing interests: